Transl. Stroke Res. (2017) 8:144–156
DOI 10.1007/s12975-016-0485-3

ORIGINAL ARTICLE

Intravascular Inflammation Triggers Intracerebral Activated Microglia and Contributes to Secondary Brain Injury After Experimental Subarachnoid Hemorrhage (eSAH)

Etienne Atangana[1,2] · Ulf C. Schneider[1,3] · Kinga Blecharz[1] · Salima Magrini[1] · Josephin Wagner[1] · Melina Nieminen-Kelhä[1] · Irina Kremenetskaia[1] · Frank L. Heppner[4] · Britta Engelhardt[5] · Peter Vajkoczy[1,3,6]

Received: 11 July 2016 / Revised: 11 July 2016 / Accepted: 14 July 2016 / Published online: 1 August 2016

Abstract Activation of innate immunity contributes to secondary brain injury after experimental subarachnoid hemorrhage (eSAH). Microglia accumulation and activation within the brain has recently been shown to induce neuronal cell death after eSAH. In isolated mouse brain capillaries after eSAH, we show a significantly increased gene expression for intercellular adhesion molecule-1 (ICAM-1) and P-selectin. Hence, we hypothesized that extracerebral intravascular inflammatory processes might initiate the previously reported microglia accumulation within the brain tissue. We therefore induced eSAH in knockout mice for ICAM-1 (ICAM-1$^{-/-}$) and P-selectin glycoprotein ligand-1 (PSGL-1$^{-/-}$) to find a significant decrease in neutrophil-endothelial interaction within the first 7 days after the bleeding in a chronic cranial window model. This inhibition of neutrophil recruitment to the endothelium results in significantly ameliorated microglia accumulation and neuronal cell death in knockout animals in comparison to controls. Our results suggest an outside-in activation of the CNS innate immune system at the vessel/brain interface following eSAH. Microglia cells, as part of the brain's innate immune system, are triggered by an inflammatory reaction in the microvasculature after eSAH, thus contributing to neuronal cell death. This finding offers a whole range of new research targets, as well as possible therapy options for patients suffering from eSAH.

Keywords Microglia · Inflammation · Subarachnoid hemorrhage · Delayed brain injury

Introduction

Secondary brain injury is the most relevant contributor to poor clinical outcome after aneurysmal subarachnoid hemorrhage (SAH), for patients that have overcome the acute phase of primary brain injury [1]. The concept of primary or early brain injury after SAH has been well characterized. It encompasses a sudden rise in intracranial pressure leading to a subsequent drop of cerebral perfusion, causing hypoxia and activating further downstream mechanisms [2–4]. Additionally, brain swelling, due to the irritating effect of blood in the subarachnoid space, can further aggravate the compromised perfusion deficit. Secondary brain injury includes a variety of events occurring in the time course of SAH within the first days to weeks after the bleeding. For many years, cerebral vasospasm and delayed cerebral ischemia have been thought to be the only contributors to secondary brain injury. Yet, the CONSCIOUS trials failed to show an improvement of patient's clinical outcome, despite a significant reduction of

Etienne Atangana and Ulf C. Schneider contributed equally to this work.

Electronic supplementary material The online version of this article (doi:10.1007/s12975-016-0485-3) contains supplementary material, which is available to authorized users.

✉ Peter Vajkoczy
peter.vajkoczy@charite.de

[1] Experimental Neurosurgery, Charité–Universitätsmedizin Berlin, 10117 Berlin, Germany

[2] Department of Anaesthesia and Intensive Care Medicine, Universitätsmedizin Göttingen, 37099 Göttingen, Germany

[3] Department of Neurosurgery, Charité–Universitätsmedizin Berlin, 12200 Berlin, Germany

[4] Department of Neuropathology, Charité–Universitätsmedizin Berlin, 10117 Berlin, Germany

[5] Theodor Kocher Institut, Universität Bern, 3012 Bern, Switzerland

[6] Department of Neurosurgery, Charité–Universitätsmedizin Berlin, Augustenburger Platz 1, 13353 Berlin, Germany

cerebral vasospasm [5]. Therefore, other possible mechanisms of delayed brain injury have been discussed [3, 5, 6]. Some of them include cortical spreading depolarizations (CSDs), toxic effects of hemoglobin metabolites, microthromboembolism, and the role of the blood-brain barrier (BBB) [7–11]. An activation of the innate immunity has also been hypothesized and discussed as predisposal for cerebral vasospasm or aneurysm formation and rupture [11–15].

In a recent work, our group has shown that SAH leads to an intracerebral accumulation of microglia, which was found to contribute significantly to neuronal cell death and which we have described as *cerebral spreading inflammation* [16]. An inflammatory milieu in the subarachnoid space after SAH has also been well characterized by our group and others [17–20]. In the CSF of patients experiencing SAH, we found a predominantly pro-inflammatory profile, comprising an upregulation of specific inflammatory cytokines and cell adhesion molecules, which play a role in leukocyte-endothelial interaction and transmigration [19]. Furthermore, using microdialysis, we have shown that the observed subarachnoid inflammation extended to the intraparenchymal compartment [21]. The mechanisms initiating the activation of the CNS innate immunity (microglia cells) have not been characterized so far. Therefore, we hypothesized that the trigger factors reside outside of the brain parenchyma, possibly in the cerebral vasculature, and lead to an activation of the innate immune system in an outside-in fashion.

To determine if an intravascular inflammatory reaction precedes and/or triggers the observed microglia accumulation upon eSAH, we established a chronic cranial window model in mice. To test if we can modulate microglia accumulation and neuronal cell death by manipulating the intravascular inflammation, we used transgenic mouse strains lacking molecules involved in neutrophil recruitment at the vessel/brain interface.

Materials and Methods

Animal Experiments

All mice including littermate control animals were bread and genotyped in our laboratory animal facilities (Forschungszentrum für Experimentelle Medizin, Charité—Universitätsmedizin Berlin). Intercellular adhesion molecule-$1^{-/-}$ (ICAM-$1^{-/-}$ (Icam1^{tm1Alb})) mice, generated by deletion of the entire coding region of the ICAM-1 gene (Bullard et al. 2007), were kindly provided by D.C. Bullard (Birmingham, Alabama, USA). P-selectin glycoprotein ligand-$1^{-/-}$ (PSGL-$1^{-/-}$) C57BL/6 mice were described before [22–25].

All animals used for induction of eSAH or chronic cranial window experiments were 12–14 weeks old (total body weight app. 22–25 g) at the start of the experiments.

Experiments were performed in four groups: sham-operated littermate controls (Sham), SAH-operated littermate controls (SAH Controls), SAH-operated ICAM-$1^{-/-}$ mice (SAH ICAM-$1^{-/-}$), and SAH-operated PSGL-$1^{-/-}$ mice (SAH-PSGL-$1^{-/-}$).

Study Approval

All animal experiments were approved by the local ethics committee on animal research (Landesamt für Gesundheit und Soziales Berlin, Germany, Reg. Nos. G240/08 and G177/14) and were committed in conformity with the German law of animal protection and the National Institute of Health Guidelines for Care and Use of Laboratory Animals.

Animal Model of Experimental SAH

A filament perforation model was applied to initiate eSAH in female mice in all groups, as described elsewhere [16]. Briefly, mice were placed in supine position after induction of an intraperitoneal ketamine/xylazine anesthesia. Via a midline incision, the carotid artery was exposed. A 5-0 non-absorbable monofilament polypropylene suture (Prolene, Ethicon, Norderstedt, Germany) was introduced into the external carotid artery in a retrograde fashion and then flipped to turn anterograde into the internal carotid artery. The filament was then pushed forward to puncture the intracranial carotid bifurcation. Animals suffering from hemiparesis after the operation were excluded due to the expected occurrence of intraparenchymal hemorrhage or stroke. At the end of the experiments, the animals were perfused with ice-cold paraformaldehyde (4 %) under deep anesthesia and the brains were cryo-conserved for later immunohistochemical analysis. Sham operation included intravascular filament placement but spared the intracranial vessel puncture.

As previously shown, induction of eSAH was highly reproducible [16]. Standard hematoxylin/eosin staining ruled out intracerebral hemorrhage and territorial infarctions at 7 and 14 days after the bleeding, while iron staining proved the occurrence of eSAH at later time points, when the subarachnoid blood had already been washed out by circulation of the cerebrospinal fluid.

Isolation of Brain Vessels, Messenger RNA Isolation, and Quantitative Real-Time PCR

Brain vessel isolation was performed in Sham Control and eSAH Control mice as described elsewhere [26]. Briefly, mouse brains were separated from olfactory bulbs, cerebella, and meninges. Brains were then homogenized in DMEM (4.5 g/L glucose). Equal volumes of 32 % dextran (60–70 kDa, Sigma-Aldrich) were added and centrifuged (15 min, 4500×*g*, 4 °C). Myelin was removed, and the pellet

was resuspended in DMEM and filtered through a nylon mesh (40 μm, Millipore). The vessels were spun down to yield the final pellet. Purity of brain vessels was assessed by immunocytochemical staining for tight junction markers, known to be predominantly enriched in brain endothelial cells (claudin-5 and zonula occludens-1) [27, 28] (Suppl. Fig. S1).

RNA isolation (PureLink RNA Mini Kit, Life Technologies), cDNA synthesis (OneStep RT-PCR Kit, Qiagen), and quantitative real-time PCR (qPCR) (Premix ex Taq Perfect Real Time Kit, Takara) were performed in accordance to the manufacturers' instructions. For qPCR amplification, we used mouse and human gene-specific primers (obtained from TIB Molbiol Syntheselabor GmbH) designed using Primer Express Software (Table 1). The ABI PRISM 7300 SDS software (relative quantification study) was used to determine the cycle threshold (CT) for each reaction, and gene expression determined for each gene was normalized to expression of the endogenous housekeeping gene, glyceraldehyde phosphate dehydrogenase (GAPDH). The mean fold change in expression of target gene was calculated by calculation of ΔCT = CT Target − CT GAPDH. The relative expression intensity was then estimated by calculating 2-ΔΔCT for each sample. Specificity of PCR products was checked by melting curve analysis.

Chronic Cranial Window Model

A chronic cranial window was prepared 2 days prior to induction of eSAH in all four groups to allow for minimization of postoperative effects on intravital microscopy. Mice were fixed in a stereotactic head holder (Bilaney rodent stereotactic head holder) in a prone position under general anesthesia (ketamine 80 mg/kg and xylazine 10 mg/kg). The skull was exposed via a midline scalp incision, and a local jelly anesthetic was applied (lidocaine gel 2 %). Using a micro drill, a midline craniotomy was placed with a mean diameter of 8 mm. Then, the dura was carefully removed, avoiding injury to the sinus and bridging veins. A glass cover slip was applied and fixed with glue (Kisling Cie AG). The skin was closed over the window, and animals were observed postoperatively.

Intravital Multifluorescence Video Microscopy

Intravital microscopy was performed under general anesthesia (ketamine/xylazine as described above) in all experimental groups. Using the stereotactic head holder, the window was exposed. Fluorescein isothiocyanate (FITC)-dextran 150 (159 kDa, 2 % in saline, Sigma-Aldrich) and Rhodamin 6G (0.2 % in saline, Sigma-Aldrich) were injected via the tail vein. Leukocyte-endothelial interaction was followed within the cortical venules and recorded using a Zeiss fluorescence stereomicroscope equipped with a high-pressure mercury lamp for epi-illumination (I 2/3 bluefilter 450–490 nm; N2 greenfilter 530–560 nm). By using two dyes with different emission spectrum, the process of multistep leukocyte recuitment, i.e., rolling, sticking, and migration along the endothelium (Rhodamine 6G) as well as microhemodynamics (FITC-dextran), could be evaluated sequentially in the according observation fields by switching between the filters. The experimental observation began with a mapping of the microvascular bed of the preparation for later reassessment of the regions of interest. Five venules (diameter 20–60 μm) were randomly selected for the documentation. The quantitative analysis of the microcirculation was performed using a 10× long distance objective as well as a 20× immersion objective with magnifications of 200× and 400×, respectively.

Table 1 Genotyping protocol for ICAM-1 and PSGL-1 knockout

Strain	Primer	Name of oligo		Sequence	
ICAM-1 null	Primer A	I-null/Geno1S		ATCGCTGCTTCATCTCTAGTGC	
	Primer B	I-null/Geno2AS		TGACTACTGCCTAGTCCCCTGC	
	Primer C	puro		AGGCATGCTGGGGATGCGGT	
PSGL-1 null	Primer A	PSGL-FW4		GAGGGTAAGGAACCTTCTCTGATG	
	Primer B	PG/NREV5		TGGATGCTGGTTGGACGGTC	
	Primer C	PG/NREV2		GTCACGTCCTGCACGACGC	
Run the PCR using the following conditions					
PCR	Cycling	Denaturation	Annealing	Elongation	Products
ICAM-1$^{-/-}$	1×	94 °C, 3 min			WT 270 bps
	35×	94°c, 45 s	61 °C, 45 s	72 °C, 45 s	KO 320 bps
	1×			72 °C, 3 min	
PSGL-1$^{-/-}$	1×	94 °C, 4 min			WT 607 bps
	39×	94°c, 30 s	60 °C, 45 s	72 °C, 1 min	KO 518 bps
	1×			72 °C, 5 min	

Results analyzed using agarose gel electrophoresis: ICAM-1$^{-/-}$ 2 %, PSGL-1$^{-/-}$ 1 %

WT wild type, *KO* knocked out

Leukocyte-endothelial interaction was divided into temporarily ("rolling") and permanently adhesive ("sticking") neutrophils. Rolling was defined as a passage time of more than 20 s within the vascular segment (normalized for the diameter). Permanent adhesion was defined as sticking neutrophils that remained in one place for longer than 20 s. The latter was counted as cells per square micrometer. The area was calculated from the diameter and the length of the vessel segment (200 μm) [19, 29, 30].

Fluorescence-Activated Cell Sorting Analysis of Brain Homogenates

In a separate set of experiments, five mouse brains per group (Sham and SAH Control) were brought into suspension using the Neural Tissue Dissociation Kit (Miltenyi Biotec) according to the manufacturer's recommendations. The presence of immune cells was evaluated via fluorescence-activated cell sorting analysis (FACS) analysis (BD FACSCanto™ II, BD Bioscience, Germany), by using antibodies against CD45 and CD11b as described previously [31]. 4,6-Diamidin-2-phenylindol (DAPI; 1:100, Sigma-Aldrich) was added to exclude dead cells before samples were analyzed.

Immunofluorescence Analysis of Murine Brains

Immunofluorescence analysis of mouse brain specimens was performed in coronary sections (thickness 10 μm). Slides were incubated with primary antibodies at 4 °C overnight. Primary antibodies labeling blood vessels were anti-rat CD31 (BD Pharmingen, 1:50), anti-goat ICAM-1 (R&D Systems, 1:100), and anti-rabbit P-selectin (Bioss Antibodies, 1:100). Microglia cells were visualized by staining for ionized calcium-binding adaptor molecule-1 (Iba-1, WAKO Pure Chemical Industries, 1:250); neuronal nuclei (anti-mouse NeuN, Millipore, 1:200) staining was used to identify neurons. Lymphocyte invasion was documented by staining against CD3 (T lymphocytes) and CD19 (B lymphocytes), antibodies against which were obtained from Abcam and diluted 1:100. Neuronal cell death was detected by terminal deoxyuridine triphosphate nick-end labeling (TUNEL, ApopTag© Red In Situ Apoptosis Detection Kit, Millipore), according to the manufacturer's protocol. Secondary antibodies (all obtained from Jackson ImmunoResearch Lab), incubated for 1.5 h at room temperature, were as follows: DyLight488 donkey anti-rabbit (1:200) and FITC donkey anti-mouse (1:100). Nuclei were counterstained with DAPI-containing mounting medium (Dianova). Neuronal cell death was detected by TUNEL (ApopTag© Red In Situ Apoptosis Detection Kit, Millipore), according to the manufacturer's protocol.

For quantitative analysis, images were taken by fluorescence microscopy (Zeiss, Axio Observer Z1, Carl Zeiss, Microimaging GmbH) equipped with a digital camera (AxioCam MRc) and hard drive for later offline freeware image analysis (ImageJ.net). Immunofluorescence sections were divided into 6 to 10 high-power fields, allowing for total cell counts per brain section on three different levels of the brain (bregma, and 1.5 mm before and behind). Image acquisition of confocal microscopy was obtained with a confocal microscope (TCS SP5, Leica) using a z step of 0.1 μm and 63× 1.4 NA oil immersion objective. All images were acquired using LCF AF software (all from Leica).

Statistical Analysis

Statistical analysis was performed using GraphPad PRISM (GraphPad Software, Version 6.0). All data were analyzed by ANOVA to detect statistical differences. All values are displayed as means ± standard deviations. p values of <0.05 were considered statistically significant.

Results

Animal Experiments

The initiation of eSAH was highly standardized and reproducible throughout the groups. The overall mortality rate due to induction of the bleeding was 19 %; the mortality rate due to cranial window preparation was 6 %; the mortality of sham operation was 3 %. These rates did not differ significantly between wild-type and knockout animals and were in line with our experience in the respective procedures.

Upregulation of Adhesion Molecules in Isolated Brain Vessels After eSAH

To quantify the expression of ICAM-1 and P-selectin, both encoding molecules involved in leukocyte-endothelial interaction, brain vessels were isolated from WT mice to perform qPCR. A time-dependent upregulation of P-selectin mRNA was found until day 4 after eSAH in comparison to sham-operated mice. Also for ICAM-1, a significant overexpression was recorded on day 2 after the bleeding (Fig. 1).

Co-Localization of Adhesion Molecules with Microvessels

Upregulation of ICAM-1 and P-selectin was further evaluated in coronary sections in WT animals upon eSAH applying immune-fluorescence microscopy. Increased co-localization

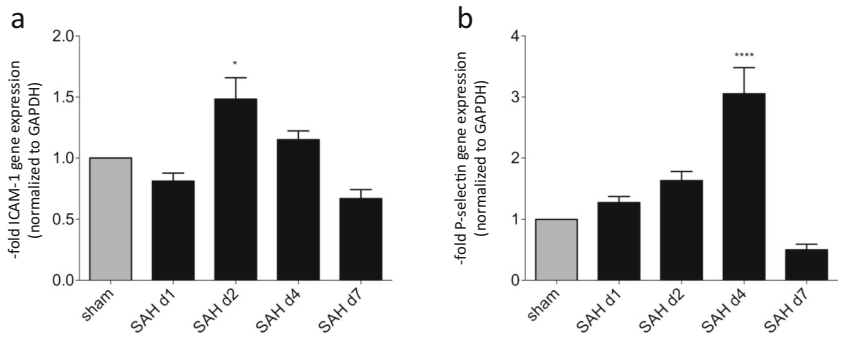

Fig. 1 In isolated brain vessels, an upregulation of ICAM-1 (**a**) and P-selectin (**b**) mRNA was found at early time points after eSAH in WT mice compared to sham-operated animals. ANOVA, $*p < 0.05$. ($n = 6$ per group and time point)

of either ICAM-1 or P-selectin with the vessel marker CD31 was detected by conventional fluorescence microscopy in comparison to sham-operated animals, where the expression of these cell adhesion molecules was much lower. This strong appearance of ICAM-1 and P-selectin after eSAH was even more clearly demonstrated by confocal microscopy (Fig. 2).

Influence of eSAH on Cerebral Microhemodynamics

Repetitive in vivo evaluation of the superficial microvasculature and the neutrophil-endothelial interaction through our chronic cranial window model was feasible throughout the observation period. The microhemodynamic parameters

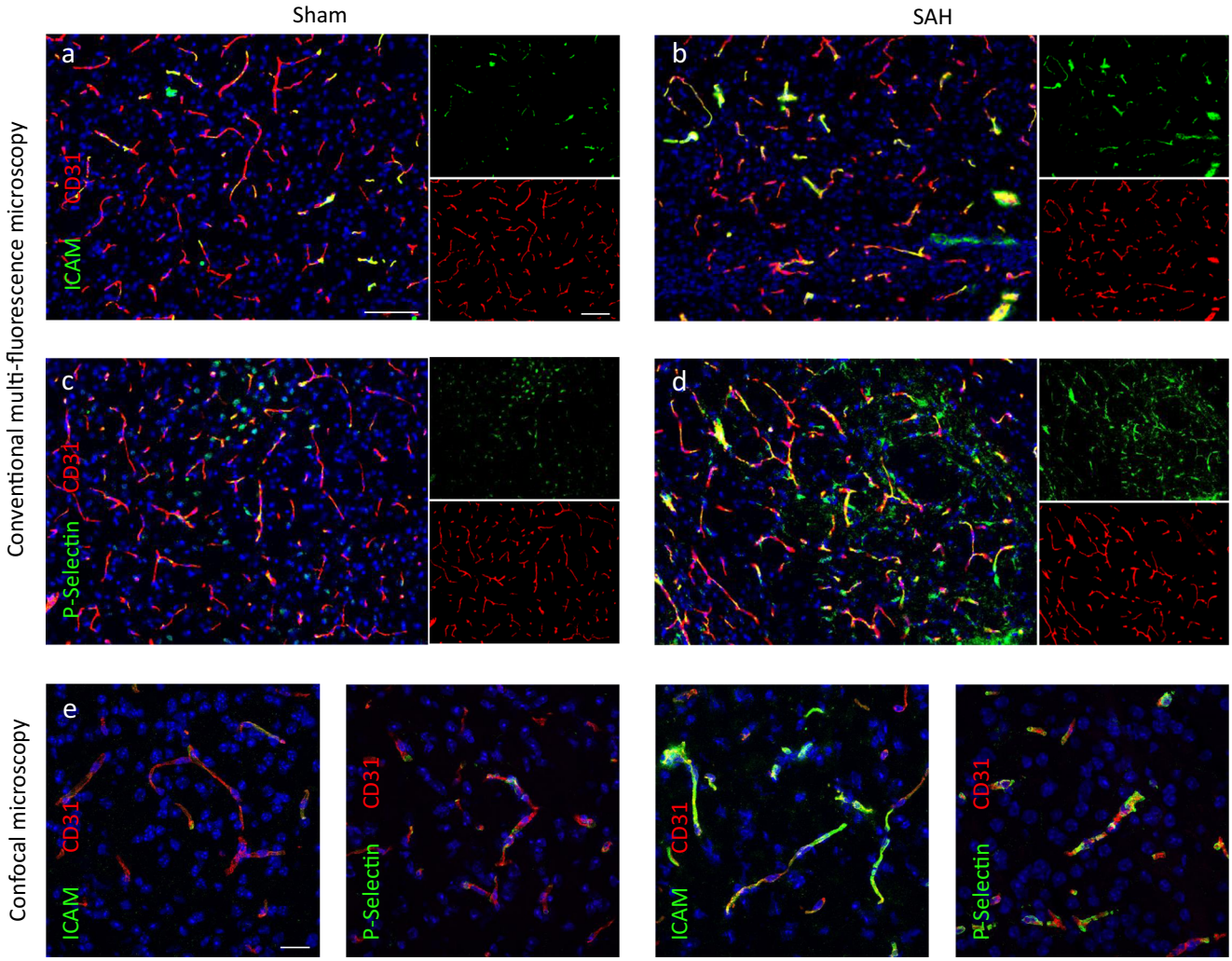

Fig. 2 In WT mice, an increased expression of ICAM-1 and P-selectin was observed after eSAH in comparison to sham-operated animals as a sign for increased leukocyte-endothelial interaction and thus for possible intravascular inflammation (**a**–**d**). In conventional multifluorescence microscopy, but even more so in representative confocal microscopy images, a close correlation with microvascular structures was observed (**e**). *Scale bars* = 100 μm in conventional multifluorescence images and 20 μm in confocal microscopy images. ($n = 6$ per group and time point)

within the analyzed vessel segments did not show statistically significant differences between the groups. Vessel lengths and diameters were comparable, and thus, the calculated vessel surfaces were comparable. In eSAH-operated animals, we did not see microvascular vasoconstriction in the analyzed time interval (until day 7 after the bleeding). Concentration of leukocytes in the tube, calculated from the absolute number of leukocytes in the respective vessel segment (cells/mm^3), was significantly higher in control animals after eSAH (Fig. 3).

eSAH Leads to Intravascular Neutrophil Activation

In sham-operated animals, no increase of intravascular inflammation was observed until day 7. In contrast, we detected an increased neutrophil-endothelial interaction after induction of eSAH in control animals (Fig. 4a, b). Circulating neutrophils either interacted briefly with (rolling) or permanently adhered to (sticking) the endothelial lining. However, neutrophil-endothelial interaction upon eSAH was significantly reduced in the cortical postcapillary venules of mice lacking either PSGL-1 or ICAM-1 (Fig. 4a, c). In PSGL-1$^{-/-}$ C57BL/6 mice, intravascular leukocyte rolling and sticking were both significantly reduced throughout the whole time course of the observation period following eSAH (Fig. 4c, left). In ICAM-1$^{-/-}$ animals, only intravascular neutrophil sticking was significantly reduced throughout the whole time course of the observation period following eSAH, while rolling was unaffected (Fig. 4c, right). These results show that neutrophils are recruited to the endothelial lining upon eSAH and that this recruitment can be suppressed by knocking out the typical cell adhesion molecules ICAM-1 and PSGL-1. They also confirm that ICAM-1 is rather used by neutrophils to arrest on the postcapillary endothelium, while they rather use PSGL-1 to roll on activated endothelium.

Leukocytes Fail to Migrate into the CNS Following eSAH

Next, we addressed the question whether leukocytes (or specific subsets) migrate into the CNS parenchyma following their activation and recruitment to the endothelium of pial blood vessels or whether they remain at the vessel/brain interface, as recently suggested for granulocyte and lymphocyte activation after ischemic stroke [32, 33]. In former studies, we already excluded monocyte/macrophage as well as granulocyte invasion into the brain [16]. Our current results did not show any upregulation of lymphocyte count as evaluated by FACS analysis (Fig. 5a) or lymphocyte migration into the brain tissue either, as evaluated by immunofluorescence staining (Fig. 5b), supporting our theory of an exclusively brain-derived immune cell-driven reaction. FACS cell populations and gating strategies are shown in Suppl. Fig. S2.

Inhibition of Intravascular Neutrophil Activation Suppresses Activation of Resident Microglia Cells

A recruitment to and activation of neutrophils at the endothelium were observed within the first days after eSAH. Next, we showed that neutrophil recruitment to the vessel/brain interface was followed by accumulation of microglia cells, as demonstrated by an increased Iba-1 immunofluorescence, in brain cryo-sections of control animals 7 and 14 days after

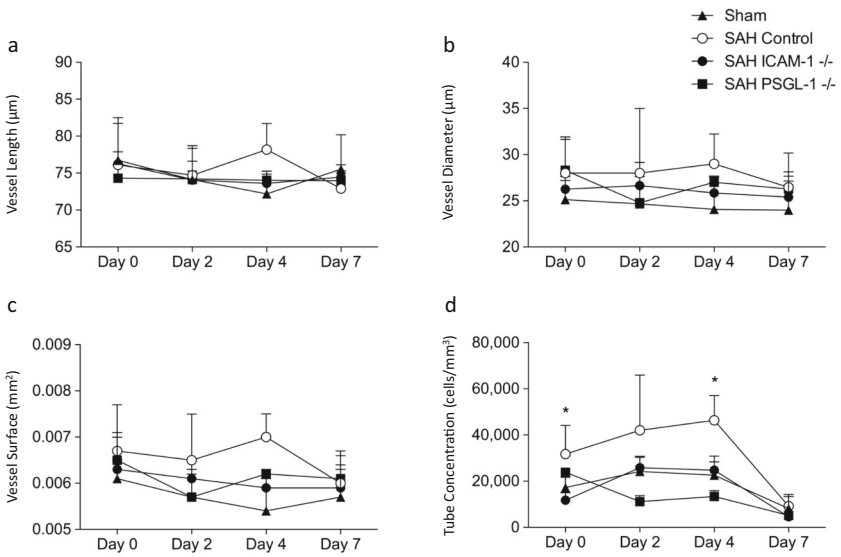

Fig. 3 The standard microhemodynamic parameters, observed through our chronic cranial windows, did not differ significantly between the four groups. Vessel length and diameter showed comparable values. Especially, no microvascular vasospastic events were documented throughout the observation period until day 7 (**a**, **b**). The vascular surface (mm^2) was calculated from these first two values without showing significant differences (**c**). Only the leukocyte tube concentration (cells/mm^3) showed higher absolute values after eSAH in control animals (**d**). ($n = 4$ per group, repetitive measurements)

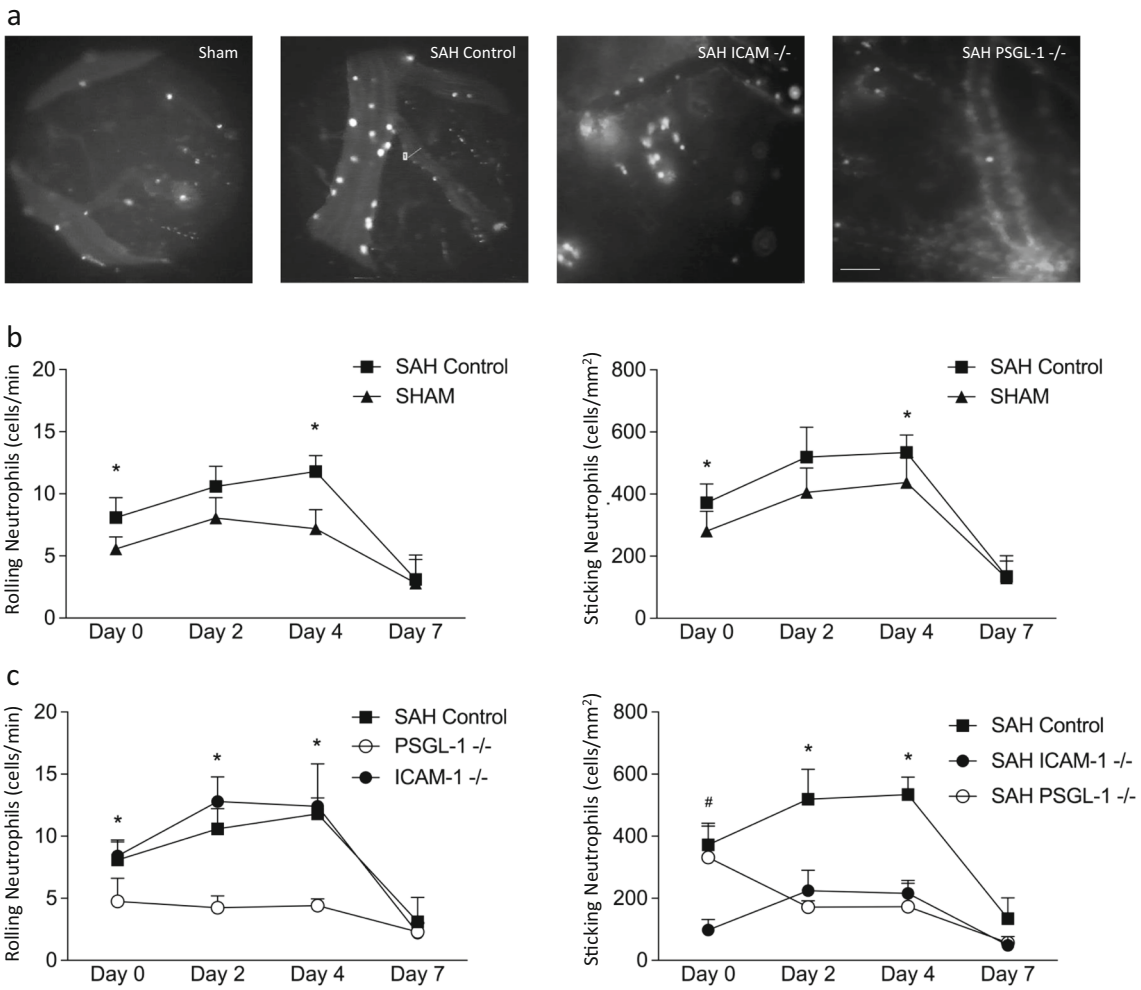

Fig. 4 Intravascular activation of neutrophil-endothelial interaction was seen upon eSAH in repeated intravital multifluorescence video microscopy through a chronic cranial window. Representative intravital microscopy images of the four groups show significantly more fluorescence-marked leukocytes in the vascular lumen (*white dots*) in WT animals upon eSAH, when compared to the other groups (**a**, *scale bar* = 60 μm). More rolling and sticking neutrophils were found in the cortical venules from day 0 to day 4 after the hemorrhage in comparison to control animals (**b**). In PSGL-$1^{-/-}$ C57BL/6 mice, rolling and sticking activity of circulating neutrophils in the cortical venules was significantly reduced after eSAH in comparison to control mice. In ICAM-$1^{-/-}$ C57BL/6 mice, only the number of sticking neutrophils was significantly lower when compared to control mice after eSAH (**c**). ANOVA, $*p < 0.05$. ($n = 4$ per group, repetitive measurements)

eSAH (Fig. 6a–b, e). This activation of microglia cells was comparable in localization and extent to the cerebral spreading inflammation described in our recent work [16]. In both PSGL-$1^{-/-}$ and ICAM-$1^{-/-}$ C57BL/6 mice, the reduction of intravascular inflammation was accompanied by a significant suppression of eSAH-induced accumulation of activated microglia in the brain parenchyma (Fig. 6c–d, e).

Attenuation of Neuronal Cell Death

We have previously shown that the accumulation of microglia as part of the CNS innate immune system results in increased neuronal cell death following eSAH. Thus, we investigated TUNEL positivity in NeuN cells in PSGL-$1^{-/-}$ an ICAM-$1^{-/-}$ C57BL/6 mice on days 7 and 14 after eSAH. In contrast to sham-operated controls, we found a significantly higher number of neurons positively stained for TUNEL in eSAH-operated controls confirming increased neuronal cell death after eSAH (Fig. 7a–b, e). Inhibition of intravascular inflammation in both PSGL-$1^{-/-}$ and ICAM-$1^{-/-}$ C57BL/6 mice significantly reduced neuronal cell death after eSAH (Fig. 7c–e).

Discussion

In this study, we observed an overexpression of adhesion molecules in cerebral microvessels after eSAH. Based on this

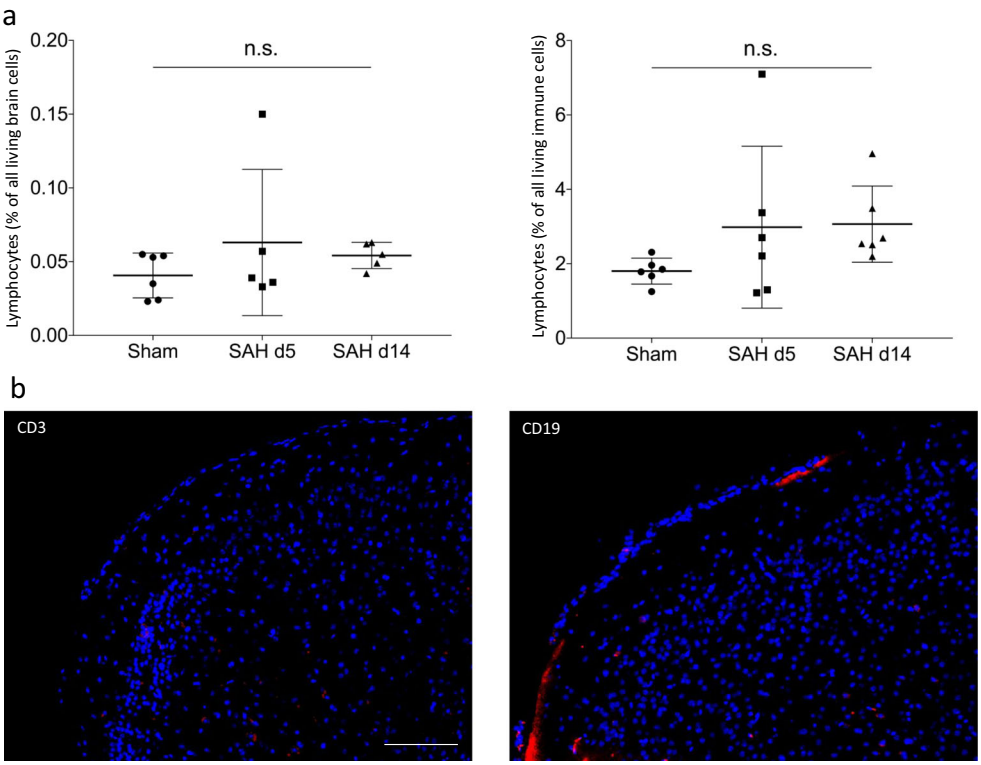

Fig. 5 FACS analysis of brain homogenates showing relative changes in the number of lymphocytes upon eSAH. Neither in relation to all living brain cells (**a**, *left*) nor in relation to all CD45+ cells, representing the immune cell population (**a**, *right*), a significant change in the proportion of lymphocytes was found 5 or 14 days after the bleeding in comparison to sham-operated animals. To rule out lymphocyte infiltration into the brain parenchyma, additional immunofluorescence staining for CD3 (T lymphocytes) and CD19 (B lymphocytes) was performed on a single animal basis. Representative images are displayed and show no infiltration of lymphocytes (**b**). (*Scale bar* 100 μm). ANOVA n.s. ($n = 5$ per group and time point)

finding, we tested the hypothesis if the previously described cerebral spreading inflammation, mediated by microglia is triggered outside the brain parenchyma in the cerebral vasculature. We found that eSAH results in early intravascular inflammation with recruitment of circulating neutrophils to the vessel/brain interface followed by microglia accumulation as part of the CNS innate immune system which then induces neuronal cell death within 14 days after hemorrhage (summarized in Fig. 8). Inhibition of neutrophil-endothelial interaction using mouse models lacking ICAM-1 or PSGL-1 markedly diminished the activation of the CNS innate immune system and neuronal cell death and, thus, reduced secondary brain injury after eSAH. Our data suggest that activation of circulating inflammatory cells initiates microglia-mediated cerebral spreading inflammation in an outside-in fashion following eSAH.

The cerebral vasculature and its interface to the brain, therefore, seem to be the site of initiation of the CNS immune response after eSAH. Our analysis of parameters reflecting cortical microhemodynamics by applying epi-fluorescence time-lapse video microscopy through a chronic cranial window did not reveal perfusion failure or spasm at the precapillary level until day 7 after eSAH. This ruled out that secondary changes in the brain microcirculation after eSAH contribute to brain injury or affect intravascular or intraparenchymal inflammation.

Long-term clinical outcome in patients after SAH often remains highly compromised, even though focal morphological correlates (e.g., territorial infarctions, intracerebral hemorrhage) might not be visible on imaging studies. Many patients suffer from neuropsychological deficiencies or subtle mental impairment. In previous studies, we showed that SAH induces microglia accumulation in human brains that can be clearly correlated with the clinical course [16]. Moreover, imaging studies revealed a loss of total brain volume as well as hippocampal volume in response to the bleeding [34–36]. Activation of microglia cells followed by the loss of neuronal density might therefore be considered as a possible contributor to this phenomenon. This hypothesis is strengthened by a recent finding showing neuronal loss upon microglia activation in murine hippocampi after SAH [37]. Therefore, interacting with initiation, progression, and resolution of the activation of innate immunity might provide further interesting research targets.

Several concepts of secondary brain injury have been described in the past. Besides cerebral vasospasm and inflammation, cortical spreading depolarizations or a breakdown of the autoregulatory competence of the CNS have been discussed in this context [8, 38, 39]. Furthermore, the BBB has become a research target as its breakdown was shown to be involved in brain injury after SAH [9, 40–42]. Loss of BBB function would also confirm our chain of argumentation by mediating the inflammatory processes from the vasculature into the brain parenchyma.

Several studies that considered inflammatory changes after SAH have been reported earlier. First of all, a systemic

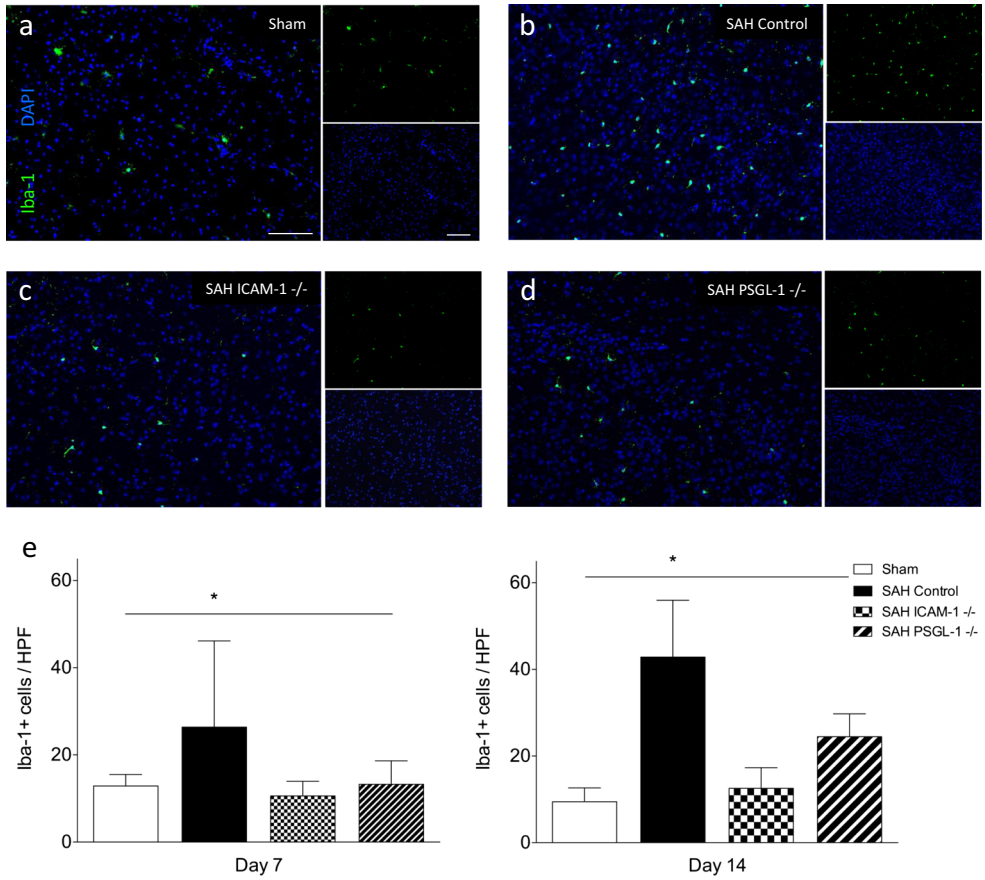

Fig. 6 eSAH lead to microglia accumulation within the brain. Representative immunofluorescence images show a limited number of Iba-1-positive cells in sham-operated animals (**a**), while in mice suffering from eSAH, an intracerebral microglia accumulation was seen in various brain regions (**b**). In ICAM-$1^{-/-}$ as well as PSGL-$1^{-/-}$ animals after eSAH, the number of Iba-1-positive microglia appeared to be markedly lower than in WT animals (**c**, **d**). Counting of the Iba-1-positive cells in various brain regions verified these imaging results, showing significantly higher numbers of microglia within the brain tissue 7 and 14 days after the bleeding in control mice. In ICAM-$1^{-/-}$, the number of microglia in the brain upon eSAH was reduced by app. 50 % on day 7 and by app. two thirds on day 14 after the bleeding, thus not being significantly different from sham-operated animals. In PSGL-$1^{-/-}$ animals compared to WT animals after eSAH, the number of intracerebral microglia was halved at both time points, as well not being higher than in sham-operated mice (**e**). *Scale bars* = 100 μm for conventional multifluorescence microscopy and 20 μm for confocal microscopy, ANOVA, $*p < 0.05$. ($n = 5$ per group and time point)

inflammatory response was documented upon SAH, the intensity of which was predictive for the clinical outcome. Here, the peripheral platelet and leukocyte count had been of predictive relevance [43, 44]. Based on our previous findings showing that cerebral spreading inflammation occurs via microglia accumulation within the brain tissue following SAH triggering neuronal cell death post SAH, we hypothesized a potential mechanism of microglia activation outside the brain parenchyma within the cerebral microvasculature, where these increased platelet and leukocyte counts take effect [16].

To test this hypothesis, we used two mouse models, one of which was deficient for ICAM-1 and the other lacking the ligand of P-selectin, PSGL-1. Both molecules are known to be critically involved in different steps of leukocyte-endothelial interactions. In general, neutrophil recruitment to the endothelium is a multistep process, in which PSGL-1 expressed on the surface of neutrophils is involved in slowing down their circulation by interacting with endothelial P-selectin (rolling), and ICAM-1 that is expressed by endothelial cells mediates firm arrest by involving lymphocyte function antigen-1 (LFA-1) expressed by different leukocyte subsets (sticking). While sticking was impaired in ICAM-$1^{-/-}$ mice, we observed impaired rolling in PSGL-$1^{-/-}$ mice. These findings are thus in accordance with the current concept that rolling is mainly attributed to PSGL-1/P-selectin interaction, while sticking is mediated by ICAM-1 and various integrins such as LFA-1 and CD11b [45, 46].

Both, rolling and sticking at or to the endothelial lining are mechanisms of neutrophil action and thus part of the innate immune system. Another, comparably complex but completely differently mediated mechanism is adopted immunity. The involvement of the latter in our newly described cerebral spreading inflammation after SAH has not yet been shown, nor excluded. The major effector cell of adopted immunity is lymphocytes, which circulate along with neutrophils, are activated by completely different mechanisms, but can also

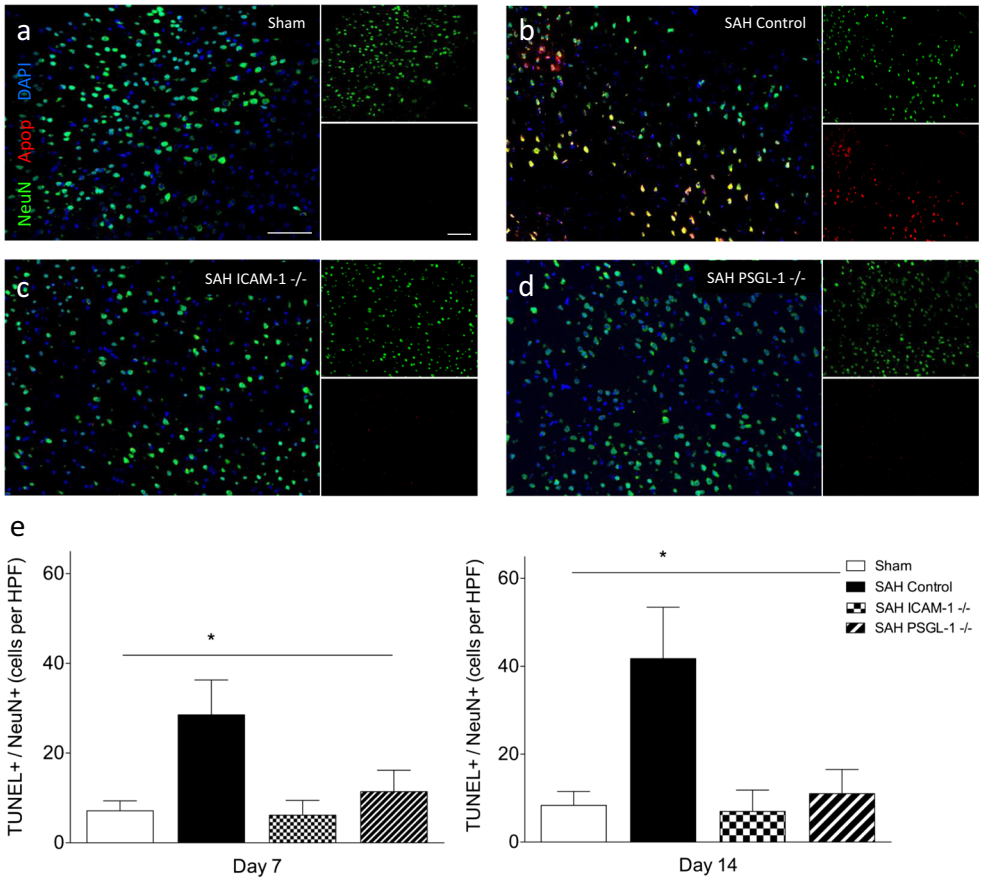

Fig. 7 eSAH induced neuronal cell death. Almost no TUNEL-positive (*red*) cells were detected in sham-operated animals, while in cortical areas, neuronal staining (*NeuN*, *green*) was regularly expressed (**a**). In brains of WT mice after eSAH, a high number of NeuN-positive cells also showed TUNEL positivity, representing neuronal cell death (*yellow*) (**b**). Neuronal cell death was markedly reduced in ICAM-1$^{-/-}$ and PSGL-1$^{-/-}$ animals in comparison to WT mice after eSAH (**c**, **d**; **a**–**d** show representative images from day 14). The absolute number of dying neurons upon eSAH in WT animals was significantly higher than in sham-operated controls on day 7 as well as on day 14 after the bleeding. In ICAM-1$^{-/-}$ mice, the number of dying neurons upon eSAH was reduced by app. 80 % at both time points, when compared to WT animals after eSAH. In PSGL-1$^{-/-}$ mice, on day 7 after the bleeding, the number of dying neurons was only half as high as in WT in control animals upon eSAH; on day 14, it was reduced by two thirds, thus not being significantly higher than in sham-operated mice (**e**). *Scale bars* = 100 μm, ANOVA, $*p < 0.05$. ($n = 5$ per group and time point)

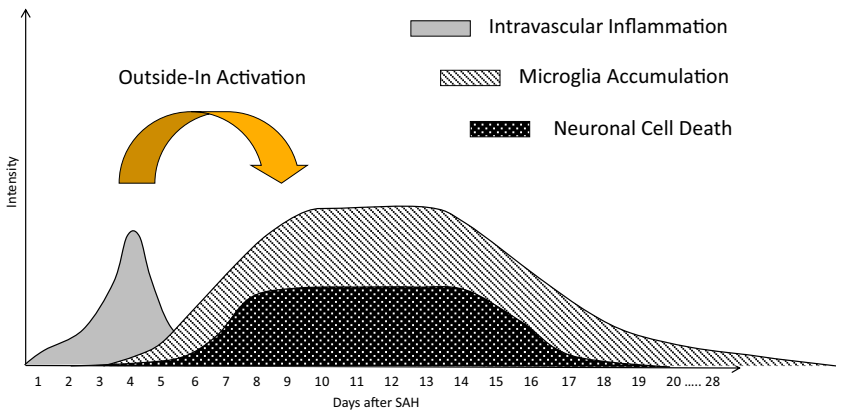

Fig. 8 Schematic illustration of our current understanding of the timeline of inflammation in the respective compartments after eSAH. Neutrophil-endothelial interaction was the first inflammatory reaction seen in our experiments, starting shortly after the bleeding and exhibiting its highest extent around day 4, acting as an outside-in activator for *the cerebral spreading inflammation*. The microglia accumulation in the brain tissue shown in the current and characterized in former studies begins around day 4 after the bleeding, climaxes around days 9–14 and fades toward day 28. Within the same time interval, neuronal cell death takes place. Both microglia accumulation as well as neuronal cell death were controllable by microglia depletion as well as inhibition of neutrophil-endothelial interaction

migrate into inflamed tissue. After having ruled out neutrophil as well as monocyte infiltration into the inflamed brain upon SAH, our current data show that also lymphocytes cannot be found within the inflamed brain tissue. This data supports and completes our former theory of a cerebral spreading inflammation, which is driven by the brain's innate immune system alone, the microglia [16]—without any infiltrating leukocytes (neither from innate, not from adopted immunity) from the periphery.

Our results are also in line with previous findings by other groups. In eSAH performed in rats, an increased immune cell trafficking within the cerebral microvasculature has been observed. Blockage of vascular adhesive protein-1 (VAP-1) caused decreased neurological impairment and a normalization of microvascular reactivity. Yet, following eSAH in rats, the authors described neutrophil infiltration into the brain, which was not observed in our experimental setup [47, 48]. This discrepancy might be explained by applying two different methods used for determination for immune cell infiltration. While in our experiments we had used a chimeric mouse model for granulocytes, monocytes, and macrophages, as well as FACS and immunofluorescence staining for different lymphocyte subsets, Xu and collaborators estimated neutrophil infiltration only, by using an index during intravital video microscopy. Thus, an extravasation (also into the subarachnoid space) cannot be differentiated from an infiltration into the brain tissue.

The question why microglia, as part of the brain's innate immune system, inflict additional injury on a prestressed brain has not been solved. A potential hypothesis is their evolution as "gatekeeper" of the CNS integrity, e.g., against infections [49, 50]. In non-infectious pathologies like cerebral ischemia or SAH, inflammatory molecules can be secreted by damaged cells as a signal of stress [51]. Activated microglia might therefore even worsen the situation by fulfilling their evolutionary designation in these pathologies. Microglia after eSAH are in a state of activation (at least several days after the bleeding), according to an upregulation of various inflammatory cytokines in isolated microglia after eSAH. The protective versus detrimental role of microglia in inflammatory CNS diseases is best characterized in models of experimental autoimmune encephalitis. Here, microglia and meningeal macrophages seem to be able to act in both ways, dependent on the actual state of the disease [52]. Also, lymphocytes and neutrophils can act in deleterious ways after certain models of brain injury. Polymorphonuclear neutrophils have been shown to contribute significantly to brain injury after cerebral ischemia [32, 51, 53–55]. The pathomechanism of SAH differs markedly from cerebral ischemia. In our model, we ruled out lymphocyte invasion into the brain parenchymal tissue by FACS and immunofluorescence stainings. The invasion of monocytes or macrophages had already been ruled out in former experiments [16].

Based on the present and former results [16], our current understanding is that an outside-in activation of the innate immune system occurs after SAH. First, the neutrophil interaction with the activated endothelium within the microvascular system followed by cerebral spreading inflammation has been observed. A recruitment of peripheral immune cells into the brain has been ruled out. The chronic cranial window allowed for an observation of the microvasculature exclusively at the dorsal surface of the brain, while microglia activation within the brain started near the skull base, at the location of the highest blood amount. Therefore, we assume that we might not have enough information about intravascular leukocyte activation at the site of bleeding. We hypothesize that it might even be more pronounced and that the propagation of inflammation around the brain occurs quickly—possibly via the Virchow-Robin spaces and subarachnoid space, in which an inflammatory milieu has been hypothesized before [16, 19, 56–58].

A variety of models for eSAH has been established. In our laboratory, the filament perforation model is the preferred technique. Although the insertion of cerebral vasculature in sham-operated animals as well, we decided to stay with the established model rather, than to produce results that might not have been comparable with our former studies. We acknowledge that by using this technique, we might underestimate the difference in intravascular inflammation between sham-operated animals and eSAH-operated animals.

Conclusion

In summary, our data show that an intravascular inflammation precedes a wave of intracerebral microglia activation that we recently described as cerebral spreading inflammation, and which inflicts neuronal cell death after eSAH. Attenuation of intravascular neutrophil-endothelial interaction led to a significant decrease of microglia accumulation and activation as well as neuronal cell death. These results uncover another mechanistic step in activation of the CNS immune system and consolidate the relevance of a neuroinflammatory response for secondary brain injury after SAH.

Acknowledgments We thank Dr. Urban Deutsch (Theodor Kocher Institute, Bern, Switzerland) for maintaining the breeding stock of the PSGL-1$^{-/-}$ and ICAM-1$^{-/-}$ C67BL/6 mice. We thank Lars Winkler (FMP Berlin Buch) for the preparation of isolated brain capillaries. We thank Dr. Susan Brandenburg for FACS analyses.

Compliance with Ethical Standards This work was supported by the Deutsche Forschungsgemeinschaft (SFB TRR 43 and NeuroCure Exc 257 to FLH and PV, as well as HE 3130/6-1 to FLH) and the Federal Ministry of Education and Research (DLR/BMBF; Kompetenznetz Degenerative Demenzen) to FLH and the Swiss Heart Foundation to BE.

Conflict of Interest Etienne Atangana has no conflict of interest.
Ulf C. Schneider has no conflict of interest.
Kinga Blecharz has no conflict of interest.
Salima Magrini has no conflict of interest.
Josephin Wagner has no conflict of interest.
Melina Nieminen-Kelhä has no conflict of interest.
Irina Kremenetskaia has no conflict of interest.
Frank Heppner has no conflict of interest.
Britta Engelhardt has no conflict of interest.
Peter Vajkoczy has no conflict of interest.

Ethical Approval All applicable international, national, and institutional guidelines for the care and use of animals were followed.

References

1. Solenski NJ, Haley EC, Kassell NF, Kongable G, Germanson T, Truskowski L, et al. Medical complications of aneurysmal subarachnoid hemorrhage: a report of the multicenter, cooperative aneurysm study. Participants of the multicenter cooperative aneurysm study. Crit Care Med. 1995;23:1007–17.
2. Chou SH-Y, Feske SK, Atherton J, Konigsberg RG, De Jager PL, Du R, et al. Early elevation of serum tumor necrosis factor-α is associated with poor outcome in subarachnoid hemorrhage. J Investig Med. 2012;60:1054–8.
3. Hansen-Schwartz J, Vajkoczy P, Macdonald RL, Pluta RM, Zhang JH. Cerebral vasospasm: looking beyond vasoconstriction. Trends Pharmacol Sci. 2007;28:252–6.
4. Hasegawa Y, Suzuki H, Sozen T, Altay O, Zhang JH. Apoptotic mechanisms for neuronal cells in early brain injury after subarachnoid hemorrhage. Acta Neurochir Suppl. 2011;110:43–8. Vienna: Springer Vienna.
5. Macdonald RL, Kassell NF, Mayer S, Ruefenacht D, Schmiedek P, Weidauer S, et al. Clazosentan to overcome neurological ischemia and infarction occurring after subarachnoid hemorrhage (CONSCIOUS-1): randomized, double-blind, placebo-controlled phase 2 dose-finding trial. Stroke. 2008;39:3015–21.
6. Macdonald RL, Higashida RT, Keller E, Mayer SA, Molyneux A, Raabe A, et al. Preventing vasospasm improves outcome after aneurysmal subarachnoid hemorrhage: rationale and design of CONSCIOUS-2 and CONSCIOUS-3 trials. Neurocrit Care. 2010;13:416–24.
7. Clark JF, Loftspring M, Wurster WL, Pyne-Geithman GJ. Chemical and biochemical oxidations in spinal fluid after subarachnoid hemorrhage. Front Biosci. 2008;13:1806–12.
8. Dreier JP, Major S, Manning A, Woitzik J, Drenckhahn C, Steinbrink J, et al. Cortical spreading ischaemia is a novel process involved in ischaemic damage in patients with aneurysmal subarachnoid haemorrhage. Brain. 2009;132:1866–81.
9. Park S, Yamaguchi M, Zhou C, Calvert JW, Tang J, Zhang JH. Neurovascular protection reduces early brain injury after subarachnoid hemorrhage. Stroke. 2004;35:2412–7.
10. Stein SC, Browne KD, Chen X-H, Smith DH, Graham DI. Thromboembolism and delayed cerebral ischemia after subarachnoid hemorrhage: an autopsy study. Neurosurgery. 2006;59:781–7. Discussion 787–8.
11. Tiebosch IACW, Dijkhuizen RM, Cobelens PM, Bouts MJRJ, Zwartbol R, van der Meide PH, et al. Effect of interferon-β on neuroinflammation, brain injury and neurological outcome after experimental subarachnoid hemorrhage. Neurocrit Care. 2013;18:96–105. Humana Press Inc.
12. Chalouhi N, Ali MS, Jabbour PM, Tjoumakaris SI, Gonzalez LF, Rosenwasser RH, et al. Biology of intracranial aneurysms: role of inflammation. J Cereb Blood Flow Metab. 2012;32:1659–76.
13. Hasan DM, Chalouhi N, Jabbour P, Dumont AS, Kung DK, Magnotta VA, et al. Evidence that acetylsalicylic acid attenuates inflammation in the walls of human cerebral aneurysms: preliminary results. J Am Heart Assoc. 2013;2:e000019. Lippincott Williams & Wilkins.
14. Provencio JJ. Inflammation in subarachnoid hemorrhage and delayed deterioration associated with vasospasm: a review. Acta Neurochir Suppl. 2013;115:233–8. Vienna: Springer Vienna.
15. Tulamo R, Frösen J, Junnikkala S, Paetau A, Pitkäniemi J, Kangasniemi M, et al. Complement activation associates with saccular cerebral artery aneurysm wall degeneration and rupture. Neurosurgery. 2006;59:1069–76. discussion 1076–7.
16. Schneider UC, Davids A-M, Brandenburg S, Müller A, Elke A, Magrini S, et al. Microglia inflict delayed brain injury after subarachnoid hemorrhage. Acta Neuropathol. 2015;130:215–31. Springer Berlin Heidelberg; 1–17.
17. Dengler J, Schefold JC, Graetz D, Meisel C, Splettstösser G, Volk H-D, et al. Point-of-care testing for interleukin-6 in cerebro spinal fluid (CSF) after subarachnoid haemorrhage. Med Sci Monit. 2008;14:BR265–8.
18. Graetz D, Nagel A, Schlenk F, Sakowitz O, Vajkoczy P, Sarrafzadeh A. High ICP as trigger of proinflammatory IL-6 cytokine activation in aneurysmal subarachnoid hemorrhage. Neurol Res. 2010;32:728–35.
19. Schneider UC, Schiffler J, Hakiy N, Horn P, Vajkoczy P. Functional analysis of Pro-inflammatory properties within the cerebrospinal fluid after subarachnoid hemorrhage in vivo and in vitro. J Neuroinflammation. 2012;9:28. BioMed Central Ltd.
20. Xie X, Wu X, Cui J, Li H, Yan X. Increase ICAM-1 and LFA-1 expression by cerebrospinal fluid of subarachnoid hemorrhage patients: involvement of TNF-α. Brain Res. 2013;1512:89–96.
21. Sarrafzadeh A, Schlenk F, Gericke C, Vajkoczy P. Relevance of cerebral interleukin-6 after aneurysmal subarachnoid hemorrhage. Neurocrit Care. 2010;13:339–46.
22. Dunne JL, Collins RG, Beaudet AL, Ballantyne CM, Ley K. Mac-1, but not LFA-1, uses intercellular adhesion molecule-1 to mediate slow leukocyte rolling in TNF-alpha-induced inflammation. J Immunol. 2003;171:6105–11.
23. Furie B, Furie BC. Leukocyte crosstalk at the vascular wall. Thromb Haemost. 1997;78:306–9.
24. Furie B, Furie BC. The molecular basis of platelet and endothelial cell interaction with neutrophils and monocytes: role of P-selectin and the P-selectin ligand, PSGL-1. Thromb Haemost. 1995;74:224–7.
25. Yang J, Furie BC, Furie B. The biology of P-selectin glycoprotein ligand-1: its role as a selectin counterreceptor in leukocyte-endothelial and leukocyte-platelet interaction. Thromb Haemost. 1999;81:1–7.
26. Del Vecchio G, Tscheik C, Tenz K, Helms HC, Winkler L, Blasig R, et al. Sodium caprate transiently opens claudin-5-containing barriers at tight junctions of epithelial and endothelial cells. Mol Pharm. 2012;9:2523–33. American Chemical Society.
27. Coisne C, Engelhardt B. Tight junctions in brain barriers during central nervous system inflammation. Antioxid Redox Signal. 2011;15:1285–303. Mary Ann Liebert, Inc. 140 Huguenot Street, 3rd Floor New Rochelle, NY 10801 USA.
28. Gumbiner BM. Cell adhesion: the molecular basis of tissue architecture and morphogenesis. Cell. 1996;84:345–57.
29. Vajkoczy P, Menger MD, Simpson E, Messmer K. Angiogenesis and vascularization of murine pancreatic islet isografts. Transplantation. 1995;60:123–7.
30. Vajkoczy P, Schilling L, Ullrich A, Schmiedek P, Menger MD. Characterization of angiogenesis and microcirculation of high-

grade glioma: an intravital multifluorescence microscopic approach in the athymic nude mouse. J Cereb Blood Flow Metab. 1998;18: 510–20.
31. Brandenburg S, Müller A, Turkowski K, Radev YT, Rot S, Schmidt C, et al. Resident microglia rather than peripheral macrophages promote vascularization in brain tumors and are source of alternative pro-angiogenic factors. Acta Neuropathol. 2016;131:365–78. Springer Berlin Heidelberg.
32. Enzmann G, Mysiorek C, Gorina R, Cheng Y-J, Ghavampour S, Hannocks M-J, et al. The neurovascular unit as a selective barrier to polymorphonuclear granulocyte (PMN) infiltration into the brain after ischemic injury. Acta Neuropathol. 2013;125:395–412. Springer-Verlag.
33. Engelhardt B, Liebner S. Novel insights into the development and maintenance of the blood-brain barrier. Cell Tissue Res. 2014;355: 687–99. Springer Berlin Heidelberg.
34. Bendel P, Koivisto T, Hänninen T, Kolehmainen A, Könönen M, Hurskainen H, et al. Subarachnoid hemorrhage is followed by temporomesial volume loss: MRI volumetric study. Neurology. 2006;67:575–82.
35. Bendel P, Koivisto T, Niskanen E, Könönen M, Aikiä M, Hänninen T, et al. Brain atrophy and neuropsychological outcome after treatment of ruptured anterior cerebral artery aneurysms: a voxel-based morphometric study. Neuroradiology. 2009;51:711–22.
36. Bendel P, Koivisto T, Aikiä M, Niskanen E, Könönen M, Hänninen T, et al. Atrophic enlargement of CSF volume after subarachnoid hemorrhage: correlation with neuropsychological outcome. AJNR Am J Neuroradiol. 2010;31:370–6.
37. Hanafy KA. The role of microglia and the TLR4 pathway in neuronal apoptosis and vasospasm after subarachnoid hemorrhage. J Neuroinflammation. 2013;10:83. BioMed Central Ltd.
38. Woitzik J, Peña-Tapia PG, Schneider UC, Vajkoczy P, Thomé C. Cortical perfusion measurement by indocyanine-green videoangiography in patients undergoing hemicraniectomy for malignant stroke. Stroke. 2006;37:1549–51.
39. Pluta RM, Hansen-Schwartz J, Dreier J, Vajkoczy P, Macdonald RL, Nishizawa S, et al. Cerebral vasospasm following subarachnoid hemorrhage: time for a new world of thought. Neurol Res. 2009;31:151–8.
40. Schoknecht K, Shalev H. Blood-brain barrier dysfunction in brain diseases: clinical experience. Epilepsia. 2012;53 Suppl 6:7–13. Blackwell Publishing Ltd.
41. Macdonald RL. Delayed neurological deterioration after subarachnoid haemorrhage. Nat Rev Neurol. 2014;10:44–58.
42. Thal SC, Sporer S, Schmid-Elsaesser R, Plesnila N, Zausinger S. Inhibition of bradykinin B2 receptors before, not after onset of experimental subarachnoid hemorrhage prevents brain edema formation and improves functional outcome. Crit Care Med. 2009;37:2228–34.
43. Dhar R, Diringer MN. The burden of the systemic inflammatory response predicts vasospasm and outcome after subarachnoid hemorrhage. Neurocrit Care. 2008;8:404–12.
44. Kasius KM, Frijns CJM, Algra A, Rinkel GJE. Association of platelet and leukocyte counts with delayed cerebral ischemia in aneurysmal subarachnoid hemorrhage. Cerebrovasc Dis. 2010;29: 576–83.
45. Sundd P, Gutierrez E, Koltsova EK, Kuwano Y, Fukuda S, Pospieszalska MK, et al. "Slings" enable neutrophil rolling at high shear. Nature. 2012;488:399–403. Nature Publishing Group.
46. Kuwano Y, Spelten O, Zhang H, Ley K, Zarbock A. Rolling on E- or P-selectin induces the extended but not high-affinity conformation of LFA-1 in neutrophils. Blood. 2010;116:617–24.
47. Xu H-L, Garcia M, Testai F, Vetri F, Barabanova A, Pelligrino DA, et al. Pharmacologic blockade of vascular adhesion protein-1 lessens neurologic dysfunction in rats subjected to subarachnoid hemorrhage. Brain Res. 2014;1586:83–9.
48. Xu H, Testai FD, Valyi-Nagy T, Pavuluri NM, Zhai F, Nanegrungsunk D, et al. VAP-1 blockade prevents subarachnoid hemorrhage-associated cerebrovascular dilating dysfunction via repression of a neutrophil recruitment-related mechanism. Brain Res. 2015;1603:141–9.
49. Smithason S, Moore SK, Provencio JJ. Systemic administration of LPS worsens delayed deterioration associated with vasospasm after subarachnoid hemorrhage through a myeloid cell-dependent mechanism. Neurocrit Care. 2012;16:327–34. Humana Press Inc.
50. Smithason S, Moore SK, Provencio JJ. Low-dose lipopolysaccharide injection prior to subarachnoid hemorrhage modulates delayed deterioration associated with vasospasm in subarachnoid hemorrhage. Acta Neurochir Suppl. 2013;115:253–8. Springer Vienna.
51. Jin R, Yang G, Li G. Inflammatory mechanisms in ischemic stroke: role of inflammatory cells. J Leukoc Biol. 2010;87:779–89. Society for Leukocyte Biology.
52. Bogie JFJ, Stinissen P, Hendriks JJA. Macrophage subsets and microglia in multiple sclerosis. Acta Neuropathol. 2014;128:191–213. Springer Berlin Heidelberg.
53. Barone FC, Schmidt DB, Hillegass LM, Price WJ, White RF, Feuerstein GZ, et al. Reperfusion increases neutrophils and leukotriene B4 receptor binding in rat focal ischemia. Stroke. 1992;23: 1337–47. discussion 1347–8.
54. Garcia JH, Liu KF, Yoshida Y, Lian J, Chen S, del Zoppo GJ. Influx of leukocytes and platelets in an evolving brain infarct (Wistar rat). Am J Pathol. 1994;144:188–99. American Society for Investigative Pathology.
55. del Zoppo GJ. Lessons from stroke trials using anti-inflammatory approaches that have failed. Ernst Schering Res. Found. Workshop. 2004;:155–84.
56. Xin Z-L, Wu X-K, Xu J-R, Li X. Arachnoid cell involvement in the mechanism of coagulation-initiated inflammation in the subarachnoid space after subarachnoid hemorrhage. J Zhejiang Univ Sci B. 2010;11:516–23.
57. Greenhalgh AD, Rothwell NJ, Allan SM. An endovascular perforation model of subarachnoid haemorrhage in rat produces heterogeneous infarcts that increase with blood load. Translat Stroke Res. 2012;3:164–72.
58. Provencio JJ, Fu X, Siu A, Rasmussen PA, Hazen SL, Ransohoff RM. CSF neutrophils are implicated in the development of vasospasm in subarachnoid hemorrhage. Neurocrit Care. 2010;12: 244–51.